

# 1 Ensembler: Enabling high-throughput molecular simulations at the superfamily scale

2 Daniel L. Parton,<sup>1</sup> Patrick B. Grinaway,<sup>1</sup> Sonya M. Hanson,<sup>1</sup> Kyle A. Beauchamp,<sup>1</sup> and John D. Chodera<sup>1,\*</sup>

3 <sup>1</sup>*Computational Biology Program, Sloan Kettering Institute,*  
4 *Memorial Sloan Kettering Cancer Center, New York, NY 10065*

5 (Dated: June 25, 2015)

The rapidly expanding body of available genomic and protein structural data provides a rich resource for understanding protein dynamics with biomolecular simulation. While computational infrastructure has grown rapidly, simulations on an *omics* scale are not yet widespread, primarily because software infrastructure to enable simulations at this scale has not kept pace. It should now be possible to study protein dynamics across entire (super)families, exploiting both available structural biology data and conformational similarities across homologous proteins. Here, we present a new tool for enabling high-throughput simulation in the genomics era. **Ensembler** takes any set of sequences—from a single sequence to an entire superfamily—and shepherds them through various stages of modeling and refinement to produce simulation-ready structures. This includes comparative modeling to all relevant PDB structures (which may span multiple conformational states of interest), reconstruction of missing loops, addition of missing atoms, culling of nearly identical structures, assignment of appropriate protonation states, solvation in explicit solvent, and refinement and filtering with molecular simulation to ensure stable simulation. The output of this pipeline is an ensemble of structures ready for subsequent molecular simulations using computer clusters, supercomputers, or distributed computing projects like Folding@home. **Ensembler** thus automates much of the time-consuming process of preparing protein models suitable for simulation, while allowing scalability up to entire superfamilies. A particular advantage of this approach can be found in the construction of kinetic models of conformational dynamics—such as Markov state models (MSMs)—which benefit from a diverse array of initial configurations that span the accessible conformational states to aid sampling. We demonstrate the power of this approach by constructing models for all catalytic domains in the human tyrosine kinase family, using all available kinase catalytic domain structures from any organism as structural templates.

**Ensembler** is free and open source software licensed under the GNU General Public License (GPL) v2. It is compatible with Linux and OS X. The latest release can be installed via the `conda` package manager, and the latest source can be downloaded from <https://github.com/choderalab/enssembler>.

*Keywords: molecular dynamics simulation; comparative modeling; distributed simulation*

## 6 I. INTRODUCTION

7 Recent advances in genomics and structural biology have  
8 helped generate an enormous wealth of protein data at  
9 the level of amino-acid sequence and three-dimensional  
10 structure. However, proteins typically exist as an ensemble  
11 of thermally accessible conformational states, and static  
12 structures provide only a snapshot of their rich dynamical  
13 behavior. Many functional properties—such as the  
14 ability to bind small molecules or interact with signaling  
15 partners—require transitions between states, encompassing  
16 anything from reorganization of sidechains at binding inter-  
17 faces to domain motions to large scale folding-unfolding  
18 events. Drug discovery could also benefit from a more exten-  
19 sive consideration of protein dynamics, whereby small  
20 molecules might be selected based on their predicted abil-  
21 ity to bind and trap a protein target in an inactive state [1].

22 Molecular dynamics (MD) simulations have the capabil-  
23 ity, in principle, to describe the time evolution of a pro-  
24 tein in atomistic detail, and have proven themselves to be  
25 a useful tool in the study of protein dynamics. A number  
26 of mature software packages and forcefields are now avail-  
27 able, and much recent progress has been driven by advan-  
28 ces in computing architecture. For example, many MD

29 packages are now able to exploit GPUs [2, 3], which pro-  
30 vide greatly improved simulation efficiency per unit cost rel-  
31 ative to CPUs, while distributed computing platforms such  
32 as Folding@home [4], Copernicus [5, 6], and GPUGrid [7], al-  
33 low scalability on an unprecedented level. In parallel, meth-  
34 ods for building human-understandable models of protein  
35 dynamics from noisy simulation data, such as Markov state  
36 modeling (MSM) approaches, are now reaching maturity [8–  
37 10]. MSM methods in particular have the advantage of be-  
38 ing able to aggregate data from multiple independent MD  
39 trajectories, facilitating parallelization of production simu-  
40 lations and thus greatly alleviating overall computational  
41 cost. There also exist a number of mature software packages  
42 for comparative modeling of protein structures, in which a  
43 target protein sequence is modeled using one or more struc-  
44 tures as templates [11, 12].

45 However, it remains difficult for researchers to exploit the  
46 full variety of available protein sequence and structural data  
47 in simulation studies, largely due to limitations in software  
48 architecture. For example, the set up of a biomolecular sim-  
49 ulation is typically performed manually, encompassing a se-  
50 ries of fairly standard (yet time-consuming) steps such as  
51 the choice of protein sequence construct and starting struc-  
52 ture(s), addition of missing residues and atoms, solvation  
53 with explicit water and counterions (and potentially buffer  
54 components and cosolvents), choice of simulation param-  
55 eters (or parameterization schemes for components where  
56 parameters do not yet exist), system relaxation with energy

---

\* Corresponding author; [john.chodera@choderalab.org](mailto:john.chodera@choderalab.org)

57 minimization, and one or more short preparatory MD sim-  
58 ulations to equilibrate the system and relax the simulation  
59 cell. Due to the laborious and manual nature of this pro-  
60 cess, simulation studies typically consider only one or a few  
61 proteins and starting configurations. Worse still, studies (or  
62 collections of studies) that *do* consider multiple proteins of-  
63 ten suffer from the lack of consistent best practices in this  
64 preparation process, making comparisons between related  
65 proteins unnecessarily difficult.

66 The ability to fully exploit the large quantity of available  
67 protein sequence and structural data in biomolecular sim-  
68 ulation studies could open up many interesting avenues for  
69 research, enabling the study of entire protein families or su-  
70 perfamilies within a single organism or across multiple or-  
71 ganisms. The similarity between members of a given pro-  
72 tein family could be exploited to generate arrays of confor-  
73 mational models, which could be used as starting configu-  
74 rations to aid sampling in MD simulations. This approach  
75 would be highly beneficial for many MD methods, such as  
76 MSM construction, which require global coverage of the con-  
77 formational landscape to realize their full potential, and  
78 would also be particularly useful in cases where structural  
79 data is present for only a subset of the members of a pro-  
80 tein family. It would also aid in studying protein families  
81 known to have multiple metastable conformations—such as  
82 kinases—for which the combined body of structural data for  
83 the family may cover a large range of these conformations,  
84 while the available structures for any individual member  
85 might encompass only one or two distinct conformations.

86 Here, we present the first steps toward bridging the  
87 gap between biomolecular simulation software and *omics*-  
88 scale sequence and structural data: a fully automated open  
89 source framework for building simulation-ready protein  
90 models in multiple conformational substates scalable from  
91 single sequences to entire superfamilies. **Ensembler** pro-  
92 vides functions for selecting target sequences and homolo-  
93 gous template structures, and (by interfacing with a num-  
94 ber of external packages) performs pairwise alignments,  
95 comparative modeling of target-template pairs, and several  
96 stages of model refinement. As an example application, we  
97 have constructed models for the entire set of human tyro-  
98 sine kinase (TK) catalytic domains, using all available struc-  
99 tures of protein kinase domains (from any species) as tem-  
100 plates. This results in a total of almost 400,000 models,  
101 and we demonstrate that these provide wide-ranging cov-  
102 erage of known functionally relevant conformations. By us-  
103 ing these models as starting configurations for highly par-  
104 allel MD simulations, we expect their structural diversity to  
105 greatly aid in sampling of conformational space. We further  
106 suggest that models with high target-template sequence  
107 identity are the most likely to represent native metastable  
108 states, while lower sequence identity models would aid  
109 in sampling of more distant regions of accessible phase  
110 space. It is also important to note that some models (es-  
111 pecially low sequence identity models) may not represent  
112 natively accessible conformations. However, MSM meth-  
113 ods benefit from the ability to remove outlier MD trajec-  
114 tories which start from non-natively accessible conforma-

115 tions, and which would thus be unconnected with the phase  
116 space sampled in other trajectories. These methods essen-  
117 tially identify the largest subset of Markov nodes which con-  
118 stitute an ergodic network [13, 14].

119 We anticipate that **Ensembler** will prove to be useful in  
120 a number of other ways. For example, the generated mod-  
121 els could represent valuable data sets even without subse-  
122 quent production simulation, allowing exploration of the  
123 conformational diversity present within the available struc-  
124 tural data for a given protein family. Furthermore, the au-  
125 tomation of simulation set up provides an excellent oppor-  
126 tunity to make concrete certain "best practices", such as the  
127 choice of simulation parameters.

## 128 II. DESIGN AND IMPLEMENTATION

129 **Ensembler** is written in Python, and can be used via a  
130 command-line tool (`enssembler`) or via a flexible Python  
131 API to allow integration of its components into other  
132 applications. All command-line and API information in  
133 this article refers to the [version 1.0 release of Ensem-](#)  
134 [bler](#). Up-to-date documentation can be found at [ensem-](#)  
135 [bler.readthedocs.org](#).

136 The **Ensembler** modeling pipeline comprises a series of  
137 stages which are performed in a defined order. A visual  
138 overview of the pipeline is shown in Fig. 1. The various stages  
139 of this pipeline are described in detail below.

### 140 A. Target selection and retrieval

141 The first stage entails the selection of a set of *target* pro-  
142 tein sequences—the sequences for which the user is in-  
143 terested in generating simulation-ready structural models.  
144 This may be a single sequence—such as a full-length pro-  
145 tein or a construct representing a single domain—or a col-  
146 lection of sequences, such as a particular domain from an  
147 entire family of proteins. The output of this stage is a FASTA-  
148 formatted text file containing the desired target sequences  
149 with corresponding arbitrary identifiers.

150 The `enssembler` command-line tool allows targets to  
151 be selected from UniProt—a freely accessible resource for  
152 protein sequence and functional data ([uniprot.org](#)) [15]—  
153 via a UniProt search query. To retrieve target sequences  
154 from UniProt, the subcommand `gather_targets` is used  
155 with the `--query` flag followed by a UniProt query string  
156 conforming to the same syntax as the search function  
157 available on the UniProt website. For example, `--query`  
158 `'mnemonic:SRC_HUMAN'` would select the full-length hu-  
159 man Src sequence, while the query shown in Box 1 would  
160 select all human tyrosine protein kinases which have been  
161 reviewed by a human curator. In this way, the user may se-  
162 lect a single protein, many proteins, or an entire superfam-  
163 ily from UniProt. The program outputs a FASTA file, setting  
164 the UniProt mnemonic (e.g. SRC\_HUMAN) as the identifier for  
165 each target protein.

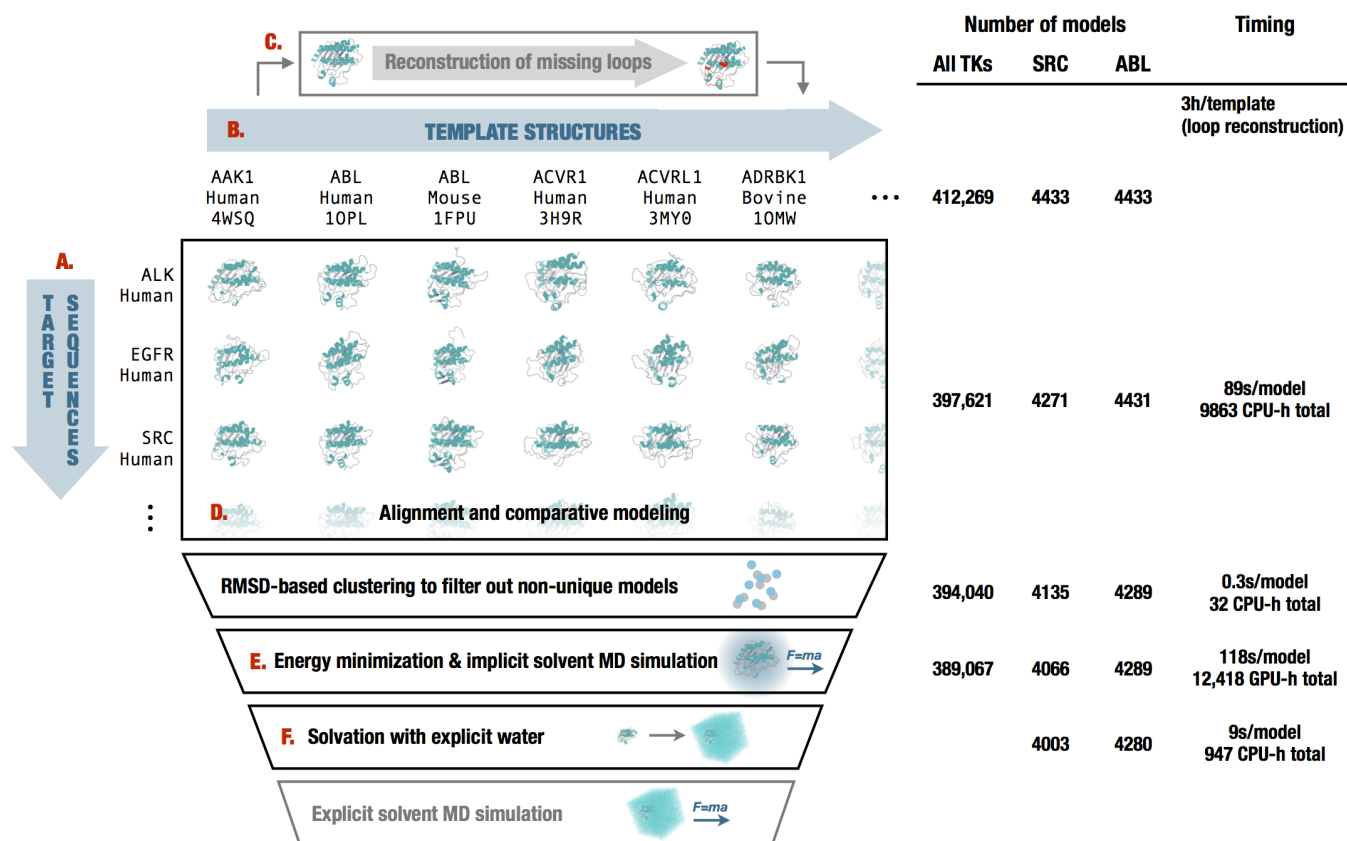


**FIG. 1. Diagrammatic representation of the stages of the Ensembler pipeline and illustrative statistics for modeling all human tyrosine kinase catalytic domains.** On the left, the various stages of the **Ensembler** pipeline are shown. The red labels indicate the corresponding text description provided for each stage in the Design and Implementation section. On the right, the number of viable models surviving each stage of the pipeline is shown for the 93 target TK domains and for two representative individual TK domains (*SRC* and *ABL*). Typical timings on a computer cluster (containing Intel Xeon E5-2665 2.4GHz hyperthreaded processors and NVIDIA GTX-680 or GTX-Titan GPUs) is reported to illustrate resource requirements per model for modeling the entire set of tyrosine kinases. Note that *CPU-h* denotes the number of hours consumed by the equivalent of a single CPU hyperthread and *GPU-h* on a single GPU—parallel execution via MPI reduces wall clock time nearly linearly.

166 In many cases, it will be desirable to build models of an  
 167 isolated protein domain, rather than the full-length pro-  
 168 tein. The `gather_targets` subcommand allows protein  
 169 domains to be selected from UniProt data by passing a regu-  
 170 lar expression string to the `--uniprot_domain_regex` flag.  
 171 For example, the above `--query` flag for selecting all hu-  
 172 man protein kinases returns UniProt entries with domain  
 173 annotations including "Protein kinase", "Protein kinase 1",  
 174 "Protein kinase 2", "Protein kinase; truncated", "Protein ki-  
 175 nase; inactive", "SH2", "SH3", etc. The regular expression  
 176 shown in Box 1 selects only domains of the first three types.  
 177 If the `--uniprot_domain_regex` flag is used, target identi-  
 178 fiers are set with the form `[UniProt mnemonic]_D[domain`  
 179 `index]`, where the latter part represents a 0-based index for  
 180 the domain—necessary because a single target protein may  
 181 contain multiple domains of interest (e.g. `JAK1_HUMAN_DO`,  
 182 `JAK1_HUMAN_D1`).

183 Target sequences can also be defined manually (or from  
 184 another program) by providing a FASTA-formatted text file  
 185 containing the desired target sequences with corresponding  
 186 arbitrary identifiers.

## B. Template selection and retrieval

188 **Ensembler** uses comparative modeling to build models,  
 189 and as such requires a set of structures to be used as tem-  
 190 plates. The second stage thus entails the selection of tem-  
 191 plates and storage of associated sequences, structures, and  
 192 identifiers. These templates can be specified manually, or  
 193 using the `enssembler gather_templates` subcommand to  
 194 automatically select templates based on a search of the  
 195 Protein Data Bank (PDB) or UniProt. A recommended ap-  
 196 proach is to select templates from UniProt which belong to  
 197 the same protein family as the targets, guaranteeing some  
 198 degree of homology between targets and templates.

199 The `enssembler gather_templates` subcommand pro-  
 200 vides methods for selecting template structures from either  
 201 UniProt or the PDB (<http://www.rcsb.org/pdb>), speci-  
 202 fied by the `--gather_from` flag. Both methods select tem-  
 203 plates at the level of PDB chains—a PDB structure contain-  
 204 ing multiple chains with identical sequence spans (e.g. for  
 205 crystal unit cells with multiple asymmetric units) would thus  
 206 give rise to multiple template structures.

207 Selection of templates from the PDB simply requires  
208 passing a list of PDB IDs as a comma-separated string,  
209 e.g. `--query 2H8H,1Y57`. Specific PDB chain IDs can  
210 optionally also be selected via the `--chainids` flag.  
211 The program retrieves structures from the PDB server,  
212 as well as associated data from the SIFTS service  
213 ([www.ebi.ac.uk/pdbe/docs/sifts](http://www.ebi.ac.uk/pdbe/docs/sifts)) [16], which provides  
214 residue-level mappings between PDB and UniProt entries.  
215 The SIFTS data is used to extract template sequences,  
216 retaining only residues which are resolved and match  
217 the equivalent residue in the UniProt sequence—non-  
218 wildtype residues are thus removed from the template  
219 structures. Furthermore, PDB chains with less than a  
220 given percentage of resolved residues (default: 70%) are  
221 filtered out. Sequences are stored in a FASTA file, with identifiers  
222 of the form `[UniProt mnemonic]_D[UniProt  
223 domain index]_[PDB ID]_[PDB chain ID]`, e.g.  
224 `SRC_HUMAN_DO_2H8H_A`. Matching residues then extracted  
225 from the original coordinate files and stored as  
226 PDB-format coordinate files.

227 Selection of templates from UniProt proceeds in a similar  
228 fashion as for target selection; the `--query` flag is used to  
229 select full-length proteins from UniProt, while the optional  
230 `--uniprot_domain_regex` flag allows selection of individual  
231 domains with a regular expression string (Box 1). The  
232 returned UniProt data for each protein includes a list of associated  
233 PDB chains and their residue spans, and this information  
234 is used to select template structures, using the same  
235 method as for template selection from the PDB. Only structures  
236 solved by X-ray crystallography or NMR are selected,  
237 thus excluding computer-generated models available from  
238 the PDB. If the `--uniprot_domain_regex` flag is used, then  
239 templates are truncated at the start and end of the domain  
240 sequence.

241 Templates can also be defined manually. Manual specification  
242 of templates simply requires storing the sequences and arbitrary  
243 identifiers in a FASTA file, and the structures as PDB-format  
244 coordinate files with filenames matching the identifiers in the  
245 sequence file. The structure residues must also match those in  
246 the sequence file.

### 247 C. Template refinement

248 Unresolved template residues can optionally be modeled  
249 into template structures with the `loopmodel` subcommand,  
250 which employs a kinematic closure algorithm provided via  
251 the `loopmodel` tool of the Rosetta software suite [17, 18].  
252 We expect that in certain cases, pre-building template loops  
253 with Rosetta `loopmodel` prior to the main modeling stage  
254 (with MODELLER) may result in improved model quality.  
255 Loop remodeling may fail for a small proportion of templates  
256 due to spatial constraints imposed by the original structure;  
257 the subsequent modeling step thus automatically uses the  
258 remodeled version of a template if available, but otherwise  
259 falls back to using the non-remodeled version. Furthermore,  
260 the Rosetta `loopmodel` program will not model missing  
261 residues at the termini of a structure—such

262 residue spans are modeled in the subsequent stage.

### 263 D. Modeling

264 In the modeling stage, structural models of the target  
265 sequence are generated from the template structures, with  
266 the goal of modeling the target in a variety of conformations  
267 that could be significantly populated under equilibrium  
268 conditions.

269 Modeling is performed using the automodel function of  
270 the MODELLER software package [19, 20] to rapidly generate  
271 a single model of the target sequence from each template  
272 structure. MODELLER uses simulated annealing cycles along  
273 with a minimal forcefield and spatial restraints—generally  
274 Gaussian interatomic probability densities extracted from the  
275 template structure with database-derived statistics determining  
276 the distribution width—to rapidly generate candidate  
277 structures of the target sequence from the provided template  
278 sequence [19, 20].

279 While MODELLER's automodel function can generate its  
280 own alignments automatically, a standalone function was  
281 preferable for reasons of programming convenience. As  
282 such, we implemented pairwise alignment functionality using  
283 the BioPython `pairwise2` module [21]—which uses a dynamic  
284 programming algorithm—with the PAM 250 scoring matrix  
285 of Gonnet *et al.* [22]. The alignments are carried out  
286 with the `align` subcommand, prior to the modeling step  
287 which is carried out with the `build_models` subcommand.  
288 The `align` subcommand also writes a list of the sequence  
289 identities for each template to a text file, and this can be  
290 used to select models from a desired range of sequence  
291 identities. The `build_models` subcommand and all subsequent  
292 pipeline functions have a `--template_seqid_cutoff` flag  
293 which can be used to select only models with sequence  
294 identities greater than the given value. We also note that  
295 alternative approaches could be used for the alignment stage.  
296 For example, multiple sequence alignment algorithms [23],  
297 allow alignments to be guided using sequence data from  
298 across the entire protein family of interest, while (multiple)  
299 structural alignment algorithms such as MODELLER's  
300 `salign` routine [19, 20], PRO-MALS3D [24], and Espresso  
301 and 3DCoffee [25, 26], can additionally exploit structural  
302 data. **Ensembler's** modular architecture facilitates the  
303 implementation of alternative alignment approaches, and we  
304 plan to implement some of these in future versions, to allow  
305 exploration of the influence of different alignment methods  
306 on model quality.

307 Models are output as PDB-format coordinate files. To  
308 minimize file storage requirements, **Ensembler** uses the  
309 Python `gzip` library to apply compression to all sizeable  
310 text files from the modeling stage onwards. The restraints  
311 used by MODELLER could potentially be used in alternative  
312 additional refinement schemes, and **Ensembler** thus provides  
313 a flag (`--write_modeller_restraints_file`) for optionally  
314 saving these restraints to file. This option is turned off by  
315 default, as the restraint files are relatively large (e.g. ~400  
316 kB per model for protein kinase domain targets), and are not

317 expected to be used by the majority of users.

### 318 Filtering of nearly identical models

319 Because **Ensembler** treats individual chains from source  
320 PDB structures as individual templates, a number of mod-  
321 els may be generated with very similar structures if these  
322 individual chains are nearly identical in conformation. For  
323 this reason, and also to allow users to select for high di-  
324 versity if they so choose, **Ensembler** provides a way to fil-  
325 ter out models that are very similar in RMSD. The `cluster`  
326 subcommand can thus be used to identify models which dif-  
327 fer from other models in terms of RMSD distance by a user-  
328 specified cutoff. Clustering is performed using the regular  
329 spatial clustering algorithm [9], as implemented in the MSM-  
330 Builder Python library [13], which uses mdtraj [27] to calcu-  
331 late RMSD (for  $C_{\alpha}$  atoms only) with a fast quaternion char-  
332 acteristic polynomial (QCP) [28–30] implementation. A min-  
333 imum distance cutoff (which defaults to 0.6 Å) is used to re-  
334 tain only a single model per cluster.

### 335 E. Refinement of models

336 A number of refinement methods have been developed to  
337 help guide comparative modeling techniques toward more  
338 "native-like" and physically consistent conformations [31,  
339 32], of which MD simulations are an important example.  
340 While long-timescale unrestrained MD simulations (on the  
341 order of 100  $\mu$ s) have been found to be ineffective for recapit-  
342 ulating native-like conformations, possibly due to forcefield  
343 issues [33], even relatively short simulations can be useful  
344 for relaxing structural elements such as sidechain orienta-  
345 tion [32].

346 **Ensembler** thus includes a refinement module, which  
347 uses short molecular dynamics simulations to refine the  
348 models built in the previous step. As well as improving  
349 model quality, this also prepares models for subsequent  
350 production MD simulation, including solvation with explicit  
351 water molecules, if desired.

352 Models are first subjected to energy minimization (using  
353 the L-BFGS algorithm [34], followed by a short molecular  
354 dynamics (MD) simulation with an implicit solvent repre-  
355 sentation. This is implemented using the OpenMM molecu-  
356 lar simulation toolkit [2], chosen for its flexible Python API,  
357 and high performance GPU-accelerated simulation code. The  
358 simulation is run for a default of 100 ps, which in our exam-  
359 ple applications has been sufficient to filter out poor models  
360 (i.e. those with atomic overlaps unresolved by energy mini-  
361 mization, which result in an unstable simulation), as well as  
362 helping to relax model conformations. As discussed in the  
363 Results section, our example application of the **Ensembler**  
364 pipeline to the human tyrosine kinase family indicated that  
365 of the models which failed implicit solvent MD refinement,  
366 the vast majority failed within the first 1 ps of simulation.

367 The simulation protocol and default parameter values  
368 have been chosen to represent current "best practices"

369 for the refinement simulations carried out here. As such,  
370 the simulation is performed using Langevin dynamics,  
371 with a default force field choice of Amber99SB-ILDN [35],  
372 along with a modified generalized Born solvent model [36]  
373 as implemented in the OpenMM package [2]. Any of  
374 the other force fields or implicit water models imple-  
375 mented in OpenMM can be specified using the `--ff` and  
376 `--water_model` flags respectively. The simulation length  
377 can also be controlled via the `--simlength` flag, and many  
378 other important simulation parameters can be controlled  
379 from either the API or CLI (via the `--api_params` flag). The  
380 default values are set as follows—timestep: 2 fs; temper-  
381 ature: 300 K; Langevin collision rate: 20  $\text{ps}^{-1}$ ; pH (used  
382 by OpenMM for protonation state assignment): 7. We also  
383 draw attention to a recent paper which indicates that lower  
384 Langevin collision rates may result in faster phase space ex-  
385 ploration [37].

### 386 F. Solvation and NPT equilibration

387 While protein-only models may be sufficient for struc-  
388 tural analysis or implicit solvent simulations, **Ensembler**  
389 also provides a stage for solvating models with explicit wa-  
390 ter and performing a round of explicit-solvent MD refine-  
391 ment/equilibration under isothermal-isobaric (NPT) condi-  
392 tions. The solvation step solvates each model for a given  
393 target with the same number of waters to facilitate the in-  
394 tegration of data from multiple simulations, which is impor-  
395 tant for methods such as the construction of MSMs. The  
396 target number of waters is selected by first solvating each  
397 model with a specified padding distance (default: 10 Å),  
398 then taking a percentile value from the distribution (default:  
399 68th percentile). This helps to prevent models with par-  
400 ticularly long, extended loops—such as those arising from  
401 template structures with unresolved termini—from impos-  
402 ing very large box sizes on the entire set of models. The  
403 TIP3P water model [38] is used by default, but any of the  
404 other explicit water models available in OpenMM, such as  
405 TIP4P-Ew [39], can be specified using the `--water_model`  
406 flag. Models are resolvated with the target number of wa-  
407 ters by first solvating with zero padding, then incrementally  
408 increasing the box size and resolvating until the target is ex-  
409 ceeded, then finally deleting sufficient waters to match the  
410 target value. The explicit solvent MD simulation is also im-  
411 plemented using OpenMM, using the Amber99SB-ILDN force  
412 field [35] and TIP3P water [38] by default. The force field,  
413 water model, and simulation length can again be specified  
414 using the `--ff`, `--water_model`, and `--simlength` flags  
415 respectively. Further simulation parameters can be con-  
416 trolled via the API or via the CLI `--api_params` flag. Pres-  
417 sure control is performed with a Monte Carlo barostat as im-  
418 plemented in OpenMM, with a default pressure of 1 atm and  
419 a period of 50 timesteps. The remaining simulation param-  
420 eters have default values set to the same as for the implicit  
421 solvent MD refinement.

## Packaging

**Ensembler** provides a packaging module which can be used to prepare models for other uses. The `package_models` subcommand currently provides functions (specified via the `--package_for` flag) for compressing models in preparation for data transfer, or for organizing them with the appropriate directory and file structure for production simulation on the distributed computing platform Folding@home [4]. The module could easily be extended to add methods for preparing models for other purposes. For example, production simulations could alternatively be run using Copernicus [5, 6]—a framework for performing parallel adaptive MD simulations—or GPUGrid [7]—a distributing computing platform which relies on computational power voluntarily donated by the owners of nondedicated GPU-equipped computers.

## Other features

### *Tracking provenance information*

To aid the user in tracking the provenance of each model, each pipeline function also outputs a metadata file, which helps to link data to the software version used to generate it (both **Ensembler** and its dependencies), and also provides timing and performance information, and other data such as hostname.

### *Rapidly modeling a single template*

For users interested in simply using **Ensembler** to rapidly generate a set of models for a single template sequence, **Ensembler** provides a command-line tool `quickmodel`, which performs the entire pipeline for a single target with a small number of templates. For larger numbers of models (such as entire protein families), modeling time is greatly reduced by using the main modeling pipeline, which is parallelized via MPI, distributing computation across each model (or across each template, in the case of the loop reconstruction code), and scaling (in a “pleasantly parallel” manner) up to the number of models generated.

## III. RESULTS

### Modeling of all human tyrosine kinase catalytic domains

As a first application of **Ensembler**, we have built models for the human TK family. TKs (and protein kinases in general) play important roles in many cellular processes and are involved in a number of types of cancer [40]. For example, a translocation between the TK Abl1 and the pseudokinase Bcr is closely associated with chronic myelogenous leukemia [41], while mutations of Src are associated with

colon, breast, prostate, lung, and pancreatic cancers [42]. Protein kinase domains are thought to have multiple accessible metastable conformation states, and much effort is directed at developing kinase inhibitor drugs which bind to and stabilize inactive conformations [43]. Kinases are thus a particularly interesting subject for study with MSM methods [44], and this approach stands to benefit greatly from the ability to exploit the full body of available genomic and structural data within the kinase family, e.g. by generating large numbers of starting configurations to be used in highly parallel MD simulation.

We selected all human TK domains annotated in UniProt as targets, and all available structures of protein kinase domains (of any species) as templates, using the commands shown in Box 1. This returned 93 target sequences and 4433 template structures, giving a total of 412,269 target-template pairs. The templates were derived from 3028 individual PDB entries and encompassed 23 different species, with 3634 template structures from human kinase constructs.

The resultant models are available as part of a supplementary dataset which can be downloaded from the Dryad Digital Repository (DOI: [10.5061/dryad.7fg32](https://doi.org/10.5061/dryad.7fg32)).

### Ensembler modeling statistics

Crystallographic structures of kinase catalytic domains generally contain a significant number of missing residues (median 11, mean 14, standard deviation 13, max 102) due to the high mobility of several loops (Fig. 2, top), with a number of these missing spans being significant in length (median 5, mean 7, standard deviation 6, max 82; Fig. 2, bottom). To reduce the reliance on the MODELLER rapid model construction stage to reconstruct very long unresolved loops, unresolved template residues were first remodeled using the `loopmodel` subcommand. Out of 3666 templates with one or more missing residues, 3134 were successfully remodeled by the Rosetta loop modeling stage (with success defined simply as program termination without error); most remodeling failures were attributable to unsatisfiable spatial constraints imposed by the original template structure. There was some correlation between remodeling failures and the number of missing residues (Fig. 2, top); templates for which remodeling failed had a median of 20 missing residues, compared to a median of 14 missing residues for templates for which remodeling was successful.

Following loop remodeling, the **Ensembler** pipeline was performed up to and including the implicit solvent MD refinement stage, which completed with 389,067 (94%) surviving models across all TKs. To obtain statistics for the solvation stage without generating a sizeable amount of coordinate data (with solvated PDB coordinate files taking up about 0.9 MB each), the `solvate` subcommand was performed for two representative individual kinases (*Src* and *Abl1*).

The number of models which survived each stage are shown in Fig. 1, indicating that the greatest attrition oc-

```

ensembl gather_targets --query 'family:"tyr protein kinase family" AND organism:"homo sapiens" AND reviewed:yes'
                        --uniprot_domain_regex '~Protein kinase(?:; truncated)(?:; inactive)'
ensembl gather_templates --gather_from uniprot --query 'domain:"Protein kinase" AND reviewed:yes'
                        --uniprot_domain_regex '~Protein kinase(?:; truncated)(?:; inactive)'
    
```

**Box 1. Ensembler command-line functions used to select targets and templates.** The commands retrieve target and template data by querying UniProt. The query string provided to the `gather_targets` command selects all human tyrosine protein kinases which have been reviewed by a curator, while the query string provided to the `gather_templates` command selects all reviewed protein kinases of any species. The `--uniprot_domain_regex` flag is used to select a subset of the domains belonging to the returned UniProt protein entries, by matching the domain annotations against a given regular expression. In this example, domains of type "Protein kinase", "Protein kinase 1", and "Protein kinase 2" were selected, while excluding many other domain types such as "Protein kinase; truncated", "Protein kinase; inactive", "SH2", "SH3", etc. Target selection simply entails the selection of sequences corresponding to each matching UniProt domain. Template selection entails the selection of the sequences and structures of any PDB entries corresponding to the matching UniProt domains.

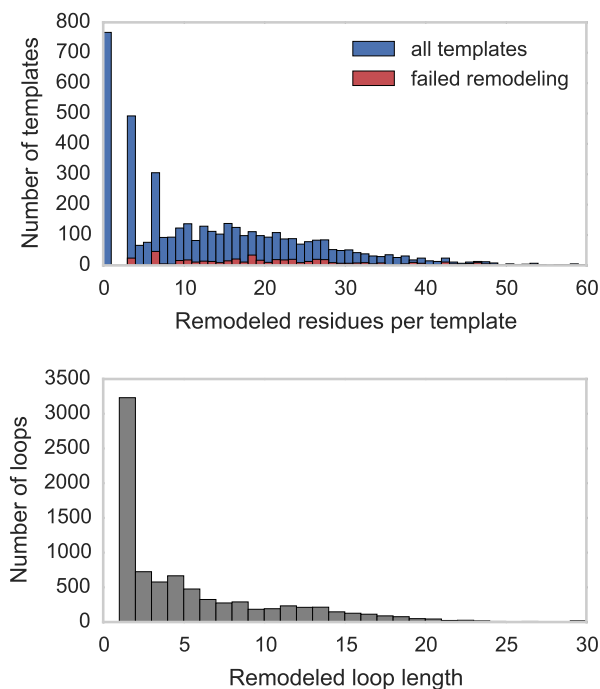


**FIG. 2. Distributions for the number of missing residues in the TK templates.** The upper histograms show the number of missing residues per template, for all templates (blue) and for only those templates for which template remodeling with the `loopmodel` subcommand failed (red). The lower histogram shows the number of residues in each missing loop, for all templates.

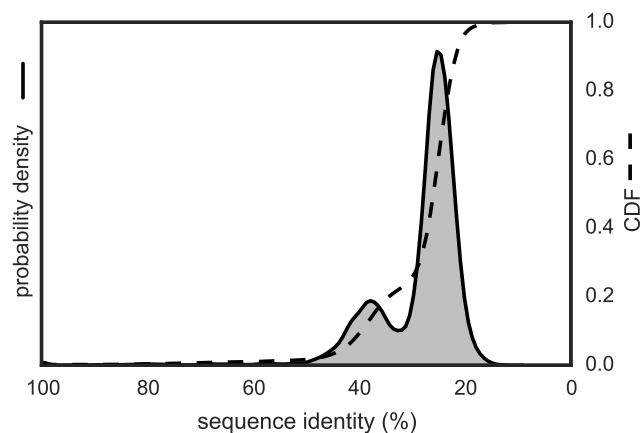


**FIG. 3. Template-target sequence identity distribution for human tyrosine kinase catalytic domains.** Sequence identities are calculated from all pairwise target-template alignments, where targets are human kinase catalytic domain sequences and templates are all kinase catalytic domains from any organism with structures in the PDB, as described in the text. A kernel density estimate of the target-template sequence identity probability density function is shown as a solid line with shaded region, while the corresponding cumulative distribution function is shown as a dashed line.

533 output from the modeling stage (without saving MODELLER  
 534 restraints files, which are about 397 kB per model) and 77 kB  
 535 for the implicit solvent MD refinement stage.

522 curred during the modeling stage. The number of refined  
 523 models for each target ranged from 4046 to 4289, with a  
 524 median of 4185, mean of 4184, and standard deviation of  
 525 57. Fig. 1 also indicates the typical timing achieved on a  
 526 cluster for each stage, showing that the `build_models` and  
 527 `refine_implicit_md` stages are by far the most compute-  
 528 intensive.

529 The files generated for each model (up to and including  
 530 the implicit solvent MD refinement stage) totaled ~116 kB in  
 531 size, totalling 0.5 GB per TK target or 42 GB for all 93 targets.  
 532 The data generated per model breaks down as 39 kB for the

## Evaluation of model quality and utility

### All tyrosine kinases

536  
 537  
 538 To evaluate the variety of template sequence similarities  
 539 relative to each target sequence, we calculated sequence  
 540 identity distributions, as shown in Fig. 3. This suggests an  
 541 intuitive division into three categories, with 355,712 mod-  
 542 els in the 0–35% sequence identity range, 51,330 models in  
 543 the 35–55% range, and 5227 models in the 55–100% range.  
 544 We then computed the RMSD distributions for the models

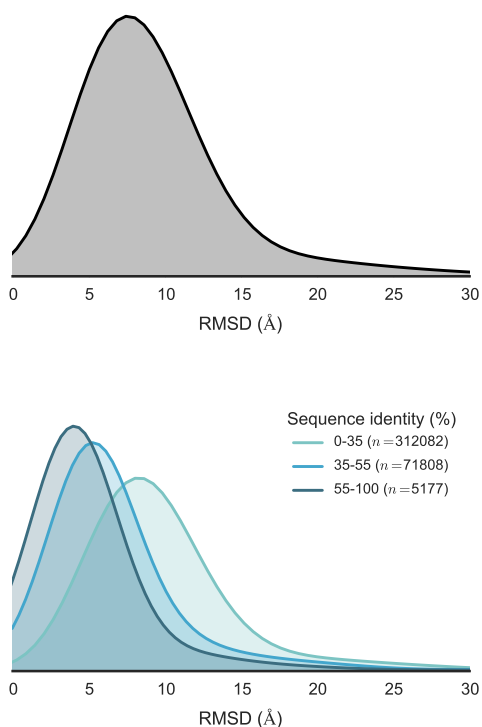


**FIG. 4. Distribution of RMSDs to all TK catalytic domain models relative to the model derived from the highest sequence identity template.** Distributions are built from data from all 93 TK domain targets. To better illustrate how conformational similarity depends on sequence identity, the lower plot illustrates the distributions as stratified into three sequence identity classes: high identity (55–100%), moderate identity (35–55%), and remote identity (0–35%). The plotted distributions have been smoothed using kernel density estimation.

545 created for each target (relative to the model derived from  
546 the template with highest sequence identity) Fig. 4, to as-  
547 sess the diversity of conformations captured by the mod-  
548 eling pipeline. Furthermore, to understand the influence  
549 of sequence identity on the conformational similarities of  
550 the resulting models, the RMSD distributions were strati-  
551 fied based on the three sequence identity categories de-  
552 scribed above. This analysis indicates that higher sequence  
553 identity templates result in models with lower RMSDs, while  
554 templates with remote sequence identities result in larger  
555 RMSDs on average.

556 We also analyzed the potential energies of the models  
557 at the end of the implicit solvent MD refinement stage.  
558 These ranged from -14180 kT to -3160 kT, with a median  
559 of -9501 kT, mean of -9418 kT, and a standard deviation  
560 of 1198 kT (with a simulation temperature of 300 K). The  
561 distributions—stratified using the same sequence identity  
562 ranges as above—are plotted in Fig. 5, indicating that higher  
563 sequence identity templates tend to result in slightly lower  
564 energy models. Of the 4973 models which failed to complete  
565 the implicit refinement MD stage, all except 9 failed within

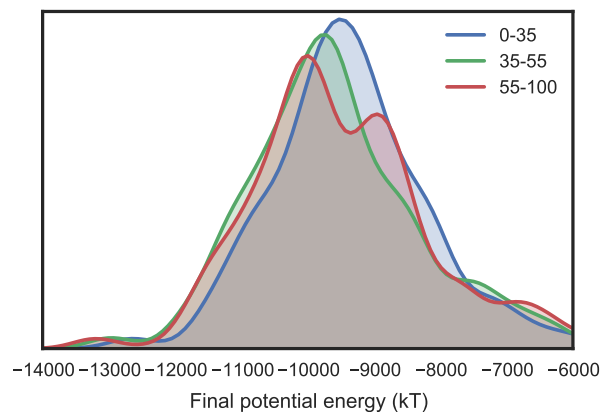


**FIG. 5. Distribution of final energies from implicit solvent MD refinement of TK catalytic domain models.** To illustrate how the energies are affected by sequence identity, the models are separated into three sequence identity classes: high identity (55–100%), moderate identity (35–55%), and remote identity (0–35%). The plotted distributions have been smoothed using kernel density estimation. Refinement simulations were carried out at the default temperature of 300 K.

566 the first 1 ps of simulation.

#### 567 *Src and Abl1*

568 To provide a more complete evaluation of the models  
569 generated, we have analyzed two example TKs (*Src* and *Abl1*)  
570 in detail. Due to their importance in cancer, these kinases  
571 have been the subject of numerous studies, encompassing  
572 many different methodologies. In terms of structural data,  
573 a large number of crystal structures have been solved (with  
574 or without ligands such as nucleotide substrate or inhibitor  
575 drugs), showing the kinases in a number of different confor-  
576 mations. These two kinases are thus also interesting targets  
577 for MSM studies, with one recent study focusing on mod-  
578 eling the states which constitute the activation pathway of  
579 *Src* [44].

580 Fig. 6 shows a superposition of a set of representative  
581 models of *Src* and *Abl1*. Models were first stratified into three  
582 ranges, based on the structure of the sequence identity dis-  
583 tribution (Fig. 3), then subjected to RMSD-based  $k$ -medoids  
584 clustering (using the *msmbuilder* clustering package [13]) to  
585 pick three representative models from each sequence iden-  
586 tity range. Each model is colored and given a transparency  
587 based on the sequence identity between the target and tem-  
588 plate sequence. The figure gives an idea of the variance  
589 present in the generated models. High sequence identity  
590 models (in opaque blue) tend to be quite structurally sim-  
591 ilar, with some variation in loops or changes in domain ori-  
592 entation.

593 The *Abl1* renderings in Fig. 6 indicate one high sequence  
594 identity model with a long unstructured region at one of  
595 the termini, which was unresolved in the original template



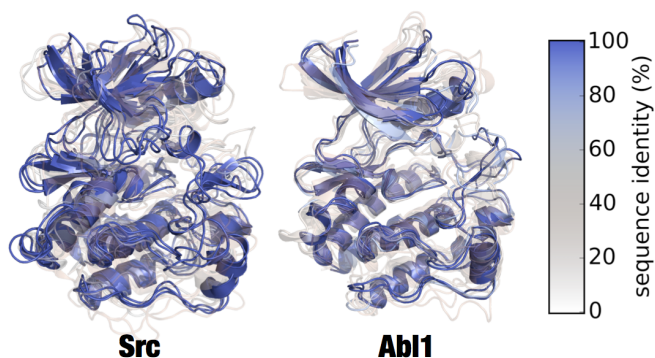


**FIG. 6. Superposition of clustered models of Src and Abl1.** Superposed renderings of nine models each for Src and Abl1, giving some indication the diversity of conformations generated by Ensembler. The models for each target were divided into three sequence identity ranges (as in Fig. 4), and RMSD-based  $k$ -medoids clustering was performed (using the msmbuilder clustering package [13]) to select three clusters from each. The models shown are the centroids of each cluster. Models are colored and given transparency based on their sequence identity, so that high sequence identity models are blue and opaque, while lower sequence identity models are transparent and red.

596 structure. While such models are not necessarily incorrect  
 597 or undesirable, it is important to be aware of the effects they  
 598 may have on production simulations performed under peri-  
 599 odic boundary conditions, as long unstructured termini can  
 600 be prone to interact with a protein's periodic image. Lower  
 601 sequence identity models (in transparent white or red) in-  
 602 dicate much greater variation in all parts of the structure.  
 603 We believe the mix of high and low sequence identity mod-  
 604 els to be particularly useful for methods such as MSM build-  
 605 ing, which require thorough sampling of the conformational  
 606 landscape. The high sequence identity models could be  
 607 considered to be the most likely to accurately represent true  
 608 metastable states. Conversely, the lower sequence identity  
 609 models could be expected to help push a simulation into re-  
 610 gions of conformation space which might take intractably  
 611 long to reach if starting a single metastable conformation.

612 To evaluate the models of *Src* and *Abl1* in the context of the  
 613 published structural biology literature on functionally rele-  
 614 vant conformations, we have focused on two residue pair  
 615 distances thought to be important for the regulation of pro-  
 616 tein kinase domain activity. We use the residue number-  
 617 ing schemes for chicken *Src* (which is commonly used in the  
 618 literature even in reference to human *Src*) [45, 46] and hu-  
 619 man *Abl1* isoform A [47–49] respectively; the exact number-  
 620 ing schemes are provided in Supporting Information S1.

621 Fig. 7 shows two structures of *Src* believed to repre-  
 622 sent inactive (PDB code: 2SRC) [45] and active (PDB code:  
 623 1Y57) [46] states. One notable feature which distinguishes  
 624 the two structures is the transfer of an electrostatic interac-  
 625 tion of E310 from R409 (in the inactive state) to K295 (in the  
 626 active state), brought about by a rotation of the  $\alpha$ C-helix.  
 627 These three residues are also well conserved [50], and a  
 628 number of experimental and simulation studies have sug-  
 629 gested that this electrostatic switching process plays a role

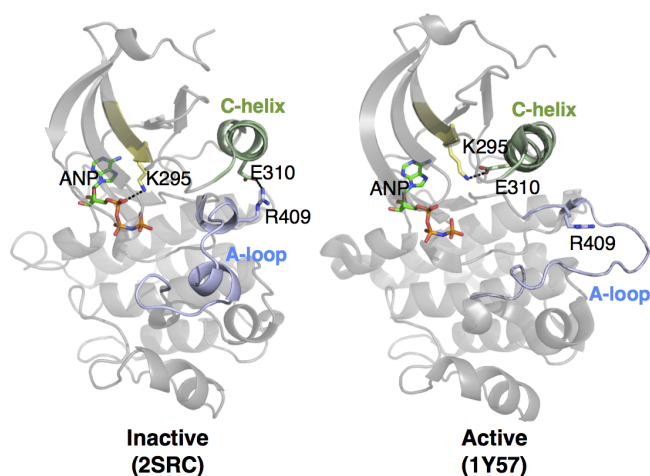


**FIG. 7. Two structures of Src, indicating certain residues in-  
 volved in activation.** In the inactive state, E310 forms a salt bridge  
 with R409. During activation, the  $\alpha$ C-helix (green) moves and ro-  
 tates, orienting E310 towards the ATP-binding site and allowing it  
 to instead form a salt bridge with K295. This positions K295 in  
 the appropriate position for catalysis. Note that ANP (phospho-  
 aminophosphonic acid-adenylate ester; an analog of ATP) is only  
 physically present in the 2SRC structure. To aid visualization of the  
 active site in 1Y57, it has been included in the rendering by struc-  
 turally aligning the surrounding homologous protein residues.

630 in a regulatory mechanism shared across the protein kinase  
 631 family [44, 51, 52]. As such, we have projected the **Ensem-**  
 632 **bler** models for *Src* and *Abl1* onto a space consisting of the  
 633 distances between these two residue pairs (Fig. 8). The mod-  
 634 els show strong coverage of regions in which either of the  
 635 electrostatic interactions is fully formed (for models across  
 636 all levels of target-template sequence identity), as well as a  
 637 wide range of regions in-between (mainly models with low  
 638 sequence identity). We thus expect that such a set of mod-  
 639 els, if used as starting configurations for highly parallel MD  
 640 simulation, could greatly aid in sampling of functionally rel-  
 641 evant conformational states.

#### 642 IV. AVAILABILITY AND FUTURE DIRECTIONS

##### 643 Availability

644 The code for **Ensembler** is hosted on the collabora-  
 645 tive open source software development platform GitHub  
 646 ([github.com/choderalab/enssembler](https://github.com/choderalab/enssembler)). The latest release can  
 647 be installed via the `conda` package manager for Python  
 648 ([conda.pydata.org](https://conda.pydata.org)), using the two commands shown in  
 649 Box 2. This will install all dependencies except for  
 650 MODELLER and Rosetta, which are not available through the  
 651 `conda` package manager, and thus must be installed sep-  
 652 arately by the user. The latest source can be downloaded  
 653 from the GitHub repository, which also contains up-to-date  
 654 instructions for building and installing the code. Documen-  
 655 tation can be found at [enssembler.readthedocs.org](https://enssembler.readthedocs.org).

656 A supplementary dataset can also be downloaded from

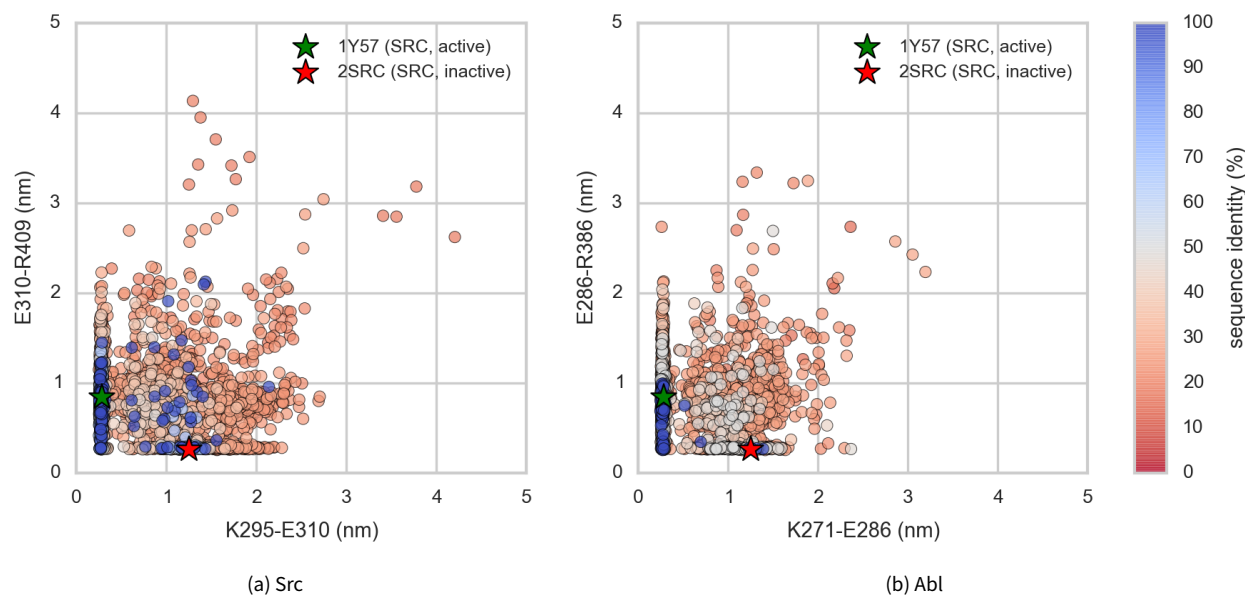


**FIG. 8. Src and Abl1 models projected onto the distances between two conserved residue pairs, colored by sequence identity.** Two Src structures (PDB entries 1Y57 [46] and 2SRC [45]) are projected onto the plots for reference, representing active and inactive states respectively. These structures and the residue pairs analyzed here are depicted in Fig. 7. Distances are measured between the center of masses of the three terminal sidechain heavy atoms of each residue. The atom names for these atoms, according to the PDB coordinate files for both reference structures, are—Lys: NZ, CD, CE (ethylamine); Glu: OE1, CD, OE2 (carboxylate); Arg: NH1, CZ, NH2 (part of guanidine).

```
conda config --add channels https://conda.binstar.org/omnia
conda install ensembler
```

### Box 2. Ensembler installation using conda.

657 the Dryad Digital Repository (DOI: [10.5061/dryad.7fg32](https://doi.org/10.5061/dryad.7fg32)).  
 658 This contains the TK models described in the III section, gen-  
 659 eral information on the targets and templates, plus a script  
 660 and instructions for regenerating the same dataset.

### Future Directions

662 Comparative protein modeling and MD simulation set-up  
 663 can be approached in a number of different ways, with vary-  
 664 ing degrees of complexity, and there are a number of obvi-  
 665 ous additions and improvements which we plan to imple-  
 666 ment in future versions of **Ensembler**.

667 Some amino acids can exist in different protonation  
 668 states, depending on pH and on their local environment.  
 669 These protonation states can have important effects on bi-  
 670 ological processes. For example, long timescale MD simula-  
 671 tions have suggested that the conformation of the DFG mo-  
 672 tif of the TK Abl1—believed to be an important regulatory  
 673 mechanism [53]—is controlled by protonation of the aspar-  
 674 tate [54]. Currently, protonation states are assigned simply  
 675 based on pH (a user-controllable parameter). At neutral pH,  
 676 histidines have two protonation states which are approxi-  
 677 mately equally likely, and in this situation the selection is

678 therefore made based on which state results in a better hy-  
 679 drogen bond. It would be highly desirable to instead use a  
 680 method which assigns amino acid protonation states based  
 681 on a rigorous assessment of the local environment. We thus  
 682 plan to implement an interface and command-line function  
 683 for assigning protonation states with MCCE2 [55–57], which  
 684 uses electrostatics calculations combined with Monte Carlo  
 685 sampling of side chain conformers to calculate pKa values.

686 Many proteins require the presence of various types of  
 687 non-protein atoms and molecules for proper function, such  
 688 as metal ions (e.g.  $Mg^{2+}$ ), cofactors (e.g. ATP) or post-  
 689 translational modifications (e.g. phosphorylation, methyla-  
 690 tion, glycosylation, etc.), and we thus plan for **Ensembler**  
 691 to eventually have the capability to include such entities  
 692 in the generated models. Binding sites for metal ions are  
 693 frequently found in proteins, often playing a role in cataly-  
 694 sis. For example, protein kinase domains contain two bind-  
 695 ing sites for divalent metal cations, and display significantly  
 696 increased activity in the presence of  $Mg^{2+}$  [58], the diva-  
 697 lent cation with highest concentration in mammalian cells.  
 698 Metal ions are often not resolved in experimental structures  
 699 of proteins, but by taking into account the full range of avail-  
 700 able structural data, it should be possible in many cases  
 701 to include metal ions based on the structures of homolo-  
 702 gous proteins. We are careful to point out, however, that  
 703 metal ion parameters in classical MD force fields have signifi-  
 704 cant limitations, particularly in their interactions with pro-  
 705 teins [59]. Cofactors and post-translational modifications  
 706 are also often not fully resolved in experimental structures,  
 707 and endogenous cofactors are frequently substituted with

708 other molecules to facilitate experimental structural analy-  
709 sis. Again, **Ensembler** could exploit structural data from a  
710 set of homologous proteins to model in these molecules, al-  
711 though there will likely be a number of challenges to over-  
712 come in the design and implementation of such functional-  
713 ity.

714 Another limitation with the present version of **Ensembler**  
715 involves the treatment of members of a protein family with  
716 especially long residue insertions or deletions. For example,  
717 the set of all human protein kinase domains listed in UniProt  
718 have a median length of 265 residues (mean 277) and a  
719 standard deviation of 45, yet the minimum and maximum  
720 lengths are 102 and 801 respectively. The latter value cor-  
721 responds to the protein kinase domain of serine/threonine-  
722 kinase *greatwall*, which includes a long insertion between  
723 the two main lobes of the catalytic domain. In principle,  
724 such insertions could be excluded from the generated mod-  
725 els, though a number of questions would arise as to how  
726 best to approach this.

## 727 Conclusion

728 We believe **Ensembler** to be an important first step to-  
729 ward enabling computational modeling and simulation of  
730 proteins on the scale of entire protein families, and suggest  
731 that it could likely prove useful for tasks beyond its original

732 aim of providing diverse starting configurations for MD sim-  
733 ulations. The code is open source and has been developed  
734 with extensibility in mind, in order to facilitate its customiza-  
735 tion for a wide range of potential uses by the wider scientific  
736 community.

## V. ACKNOWLEDGMENTS

738 The authors are grateful to Robert McGibbon (Stanford)  
739 and Arien S. Rustenburg (MSKCC) for many excellent soft-  
740 ware engineering suggestions. The authors thank Nicholas  
741 M. Levinson (University of Minnesota), Markus A. Seeliger  
742 (Stony Brook), Diwakar Shukla (Stanford), and Avner Sch-  
743 lessinger (Mount Sinai) for helpful scientific feedback on  
744 modeling kinases. The authors are grateful to Benjamin  
745 Webb and Andrej Šali (UCSF) for help with the MODELLER  
746 package, Peter Eastman and Vijay Pande (Stanford) for as-  
747 sistance with OpenMM, and Marilyn Gunner (CCNY) for assis-  
748 tance with MCCE2. All authors acknowledge support from  
749 the Sloan Kettering Institute. JDC, KAB, and DLP acknowl-  
750 edge partial support from NIH grant P30 CA008748. JDC  
751 and DLP also acknowledge the generous support of a Louis  
752 V. Gerstner Young Investigator Award. KAB was also sup-  
753 ported in part by Starr Foundation grant I8-A8-058. PBG ac-  
754 knowledges partial funding support from the Weill Cornell  
755 Graduate School of Medical Sciences.

- 
- 756 [1] G. M. Lee and C. S. Craik, *Science* **324**, 213 (2009).  
757 [2] P. Eastman, M. S. Friedrichs, J. D. Chodera, R. J. Radmer, C. M.  
758 Bruns, J. P. Ku, K. A. Beauchamp, T. J. Lane, L.-P. Wang, D.  
759 Shukla, and V. S. Pande, *J. Chem. Theory Comput.* **9**, 461  
760 (2012).  
761 [3] R. Salomon-Ferrer, A. W. Götz, D. Poole, S. L. Grand, and R. C.  
762 Walker, *J. Chem. Theor. Comput.* **9**, 3878 (2013).  
763 [4] M. Shirts and V. S. Pande, *Science* **290**, 1903 (2000).  
764 [5] S. Pronk, P. Larsson, I. Pouya, G. R. Bowman, I. S. Haque, K.  
765 Beauchamp, B. Hess, V. S. Pande, P. M. Kasson, and E. Lind-  
766 dahl, in *Proceedings of 2011 International Conference for High*  
767 *Performance Computing, Networking, Storage and Analysis, SC*  
768 *'11* (ACM, New York, NY, USA, 2011), pp. 60:1–60:10.  
769 [6] S. Pronk, I. Pouya, M. Lundborg, G. Rotskoff, B. Wesén, P. M.  
770 Kasson, and E. Lindahl, *Journal of Chemical Theory and Com-*  
771 *putation* (2015).  
772 [7] I. Buch, M. J. Harvey, T. Giorgino, D. P. Anderson, and G.  
773 De Fabritiis, *Journal of Chemical Information and Modeling*  
774 **50**, 397 (2010).  
775 [8] V. S. Pande, K. Beauchamp, and G. R. Bowman, *Methods* **52**,  
776 99 (2010).  
777 [9] J.-H. Prinz, H. Wu, M. Sarich, B. Keller, M. Fischbach, M. Held,  
778 J. D. Chodera, C. Schütte, and F. Noé, *J. Chem. Phys.* **134**,  
779 174105 (2011).  
780 [10] J. D. Chodera and F. Noé, *Curr. Opin. Struct. Biol.* **25**, 135  
781 (2014).  
782 [11] J. Moulton, K. Fidelis, A. Kryshchuk, T. Schwede, and A. Tra-  
783 montano, *Proteins: Structure, Function, and Bioinformatics*  
784 **82**, 1 (2014).  
785 [12] D. Baker and A. Šali, *Science* **294**, 93 (2001).  
786 [13] K. A. Beauchamp, G. R. Bowman, T. J. Lane, L. Maibaum, I. S.  
787 Haque, and V. S. Pande, *Journal of Chemical Theory and Com-*  
788 *putation* **7**, 3412 (2011).  
789 [14] R. Scalco and A. Caflisch, *The Journal of Physical Chemistry.*  
790 *B* **115**, 6358 (2011).  
791 [15] T. U. Consortium, *Nucleic Acids Research* **43**, D204 (2015).  
792 [16] S. Velankar, J. M. Dana, J. Jacobsen, G. van Ginkel, P. J. Gane,  
793 J. Luo, T. J. Oldfield, C. O'Donovan, M.-J. Martin, and G. J. Kley-  
794 wegt, *Nucleic Acids Research* **41**, D483 (2013).  
795 [17] B. Qian, S. Raman, R. Das, P. Bradley, A. J. McCoy, R. J. Read,  
796 and D. Baker, *Nature* **450**, 259 (2007).  
797 [18] C. Wang, P. Bradley, and D. Baker, *Journal of Molecular Biol-*  
798 *ogy* **373**, 503 (2007).  
799 [19] A. Fiser, R. K. G. Do, and A. Šali, *Protein Science* **9**, 1753 (2000).  
800 [20] A. Šali and T. L. Blundell, *Journal of Molecular Biology* **234**,  
801 779 (1993).  
802 [21] P. J. A. Cock, T. Antao, J. T. Chang, B. A. Chapman, C. J. Cox, A.  
803 Dalke, I. Friedberg, T. Hamelryck, F. Kauff, B. Wilczynski, and  
804 M. J. L. de Hoon, *Bioinformatics (Oxford, England)* **25**, 1422  
805 (2009).  
806 [22] G. H. Gonnet, M. A. Cohen, and S. A. Brenner, *Science* **256**, 1443  
807 (1992).  
808 [23] J. D. Thompson, B. Linard, O. Lecompte, and O. Poch, *PLoS*  
809 *ONE* **6**, e18093 (2011).  
810 [24] J. Pei, B.-H. Kim, and N. V. Grishin, *Nucleic Acids Research* **36**,  
811 2295 (2008).  
812 [25] F. Armougom, S. Moretti, O. Poirot, S. Audic, P. Dumas, B.  
813 Schaeli, V. Keduas, and C. Notredame, *Nucleic Acids Research*  
814 **34**, W604 (2006).

- 815 [26] O. Poirot, K. Suhre, C. Abergel, E. O'Toole, and C. Notredame, *Nucleic Acids Research* **32**, W37 (2004).  
816
- 817 [27] R. T. McGibbon, K. A. Beauchamp, C. R. Schwantes, L.-P. Wang,  
818 C. X. Hernández, M. P. Harrigan, T. J. Lane, J. M. Swails, and  
819 V. S. Pande, *bioRxiv* (2014).
- 820 [28] D. L. Theobald, *Acta Cryst. A* **61**, 478 (2005).
- 821 [29] P. Liu, D. K. Agrafiotis, and D. L. Theobald, *J. Comput. Chem.*  
822 **31**, 1561 (2010).
- 823 [30] P. Liu, D. K. Agrafiotis, and D. L. Theobald, *J. Comput. Chem.*  
824 **32**, 185 (2011).
- 825 [31] J. L. MacCallum, A. Pérez, M. J. Schnieders, L. Hua, M. P. Jacobson,  
826 and K. A. Dill, *Proteins: Structure, Function, and Bioinformatics* **79**, 74 (2011).  
827
- 828 [32] Y. Zhang, *Current Opinion in Structural Biology* **19**, 145 (2009).
- 829 [33] A. Raval, S. Piana, M. P. Eastwood, R. O. Dror, and D. E. Shaw,  
830 *Proteins: Structure, Function, and Bioinformatics* **80**, 2071  
831 (2012).
- 832 [34] D. C. Liu and J. Nocedal, *Mathematical Programming* **45**, 503  
833 (1989).
- 834 [35] K. Lindorff-Larsen, S. P. anad Kim Palmo, P. Maragakis, J. L.  
835 Klepeis, R. O. Dror, and D. E. Shaw, *Proteins* **78**, 1950 (2010).
- 836 [36] A. Onufriev, D. Bashford, and D. A. Case, *Proteins* **55**, 383  
837 (2004).
- 838 [37] J. E. Basconi and M. R. Shirts, *Journal of Chemical Theory and*  
839 *Computation* **9**, 2887 (2013).
- 840 [38] W. L. Jorgensen, J. Chandrasekhar, J. D. Madura, R. W. Impey,  
841 and M. L. Klein, *Journal of Chemical Physics* **79**, 926 (1983).
- 842 [39] H. W. Horn, W. C. Swope, J. W. Pitera, J. D. Madura, T. J.  
843 Dick, G. L. Hura, and T. Head-Gordon, *The Journal of Chemical*  
844 *Physics* **120**, 9665 (2004).
- 845 [40] D. S. Krause and R. A. Van Etten, *New England Journal of*  
846 *Medicine* **353**, 172 (2005).
- 847 [41] E. K. Greuber, P. Smith-Pearson, J. Wang, and A. M. Pendergast,  
848 *Nature Reviews Cancer* **13**, 559 (2013).
- 849 [42] L. C. Kim, L. Song, and E. B. Haura, *Nature Reviews Clinical*  
850 *Oncology* **6**, 587 (2009).
- 851 [43] Y. Liu and N. S. Gray, *Nature Chemical Biology* **2**, 358 (2006).
- 852 [44] D. Shukla, Y. Meng, B. Roux, and V. S. Pande, *Nature Commun.*  
853 **5**, 3397 (2014).
- 854 [45] W. Xu, A. Doshi, M. Lei, M. J. Eck, and S. C. Harrison, *Molecular*  
855 *Cell* **3**, 629 (1999).
- 856 [46] S. W. Cowan-Jacob, G. Fendrich, P. W. Manley, W. Jahnke, D.  
857 Fabbro, J. Liebetanz, and T. Meyer, *Structure* **13**, 861 (2005).
- 858 [47] M. A. Young, N. P. Shah, L. H. Chao, M. Seeliger, Z. V. Milanov,  
859 W. H. Biggs, D. K. Treiber, H. K. Patel, P. P. Zarrinkar, D. J. Lockhart,  
860 C. L. Sawyers, and J. Kuriyan, *Cancer Research* **66**, 1007  
861 (2006).
- 862 [48] S. W. Cowan-Jacob, G. Fendrich, A. Floersheimer, P. Furet, J.  
863 Liebetanz, G. Rummel, P. Rheinberger, M. Centeleghe, D. Fabbro,  
864 and P. W. Manley, *Acta Crystallographica Section D: Biological*  
865 *Crystallography* **63**, 80 (2006).
- 866 [49] N. M. Levinson, O. Kuchment, K. Shen, M. A. Young, M. Koldobskiy,  
867 M. Karplus, P. A. Cole, and J. Kuriyan, *PLoS Biol* **4**, e144  
868 (2006).
- 869 [50] N. Kannan and A. F. Neuwald, *Journal of Molecular Biology*  
870 **351**, 956 (2005).
- 871 [51] Z. H. Foda, Y. Shan, E. T. Kim, D. E. Shaw, and M. A. Seeliger,  
872 *Nature Communications* **6**, 5939 (2015).
- 873 [52] E. Ozkirimli, S. S. Yadav, W. T. Miller, and C. B. Post, *Protein*  
874 *Science : A Publication of the Protein Society* **17**, 1871 (2008).
- 875 [53] B. Nagar, O. Hantschel, M. A. Young, K. Scheffzek, D. Veach, W.  
876 Bornmann, B. Clarkson, G. Superti-Furga, and J. Kuriyan, *Cell*  
877 **112**, 859 (2003).
- 878 [54] Y. Shan, M. A. Seeliger, M. P. Eastwood, F. Frank, H. Xu, M. Å.  
879 Jensen, R. O. Dror, J. Kuriyan, and D. E. Shaw, *Proceedings of*  
880 *the National Academy of Sciences* **106**, 139 (2009).
- 881 [55] E. G. Alexov and M. R. Gunner, *Biophys. J.* **72**, 2075 (1997).
- 882 [56] R. E. Georgescu, E. G. Alexov, and M. R. Gunner, *Biophys. J.* **83**,  
883 1731 (2002).
- 884 [57] Y. Song, J. Mao, and M. R. Gunner, *J. Comput. Chem.* **30**, 2231  
885 (2009).
- 886 [58] J. A. Adams and S. S. Taylor, *Protein Science* **2**, 2177 (1993).
- 887 [59] S. F. Sousa, R. A. Fernandes, and M. J. Ramos, in *Kinetics*  
888 *and Dynamics: From Nano- to Bio-Scale*, Vol. 12 of *Challenges*  
889 *and Advances in Computational Chemistry and Physics*, edited  
890 by P. a. D.-D. A. Paneth (Springer Science & Business Media,  
891 Berlin, 2010), p. 530.

892

**Appendix 1: Sequences and residue numbering schemes for Src and Abl1**

893 Kinase catalytic domains are highlighted in red, and the conserved residues analyzed in the main text (Figs. 7 and 8) are  
894 highlighted with yellow background.

895

*Human Abl1 sequence*

896 1 MLEICLKLVG CKSKKGLSS SSCYLEEALQ RPVASDFEPQ GLSEARWNS KENLLAGPSE 60  
897 61 NDPNLFVALY DFVASGDNTL SITKGEKLRV LGYNHNGEWC EAQTKNGQGW VPSNYITPVN 120  
898 121 SLEKHSWYHG PVSRNAEAYL LSSGINGSFL VRESESSPGQ RSISLRYEGR VYHYRINTAS 180  
899 181 DGKLYVSSSES RFNTLAELVH HHSTVADGLI TTLHYPAPKR NKPTVYGVSP NYDKWEMERT 240  
900 241 DITMKHKLGG GQYGEVYEGV WKKYSLTVAV KTLKEDTMEV EEFLKEAAVM KEIKHPNLVQ 300  
901 301 LLGVCTREPP FYIITEFMTY GNLLDYLREC NRQEVNAVVL LYMATQISSA MEYLEKKNFI 360  
902 361 HRDLAARNCL VGENHLVKVA DFGLSRMLMTG DTYTAHAGAK FPIKWTAPES LAYNKFSIKS 420  
903 421 DVWAFGVLLW EIATYGMSPY PGIDLSQVYE LLEKDYRMER PEGCPEKVYE LMRACQWNP 480  
904 481 SDRPSFAEIH QAFETMFQES SISDEVEKEL GKQGVRGAVS TLLQAPELPT KTRTSRRAAE 540  
905 541 HRDITDVPPEM PHSKGGQGESD PLDHEPAVSP LLPRKERGPP EGGLNEDERL LPKDKKTNLF 600  
906 601 SALIKKKKKT APTPPKRSSS FREMDGQPER RGAGEEGRD ISNGALAFPT LDTADPAKSP 660  
907 661 KPSNGAGVPN GALRESGGSG FRSPHLWKKS STLTSSRLAT GEEEGGSSS KRFLRSCSAS 720  
908 721 CVPHGAKDTE WRSVTLPRDL QSTGRQFDSS TFGGHKSEKP ALPRKRAGEN RSDQVTRGTV 780  
909 781 TPPPRLVKKN EEAADDEVFKD IMESSPGSSP PNLTPKPLRR QVTVAPASGL PHKEEAGKGS 840  
910 841 ALGTPAAEP VPTPSKAGSG APGGTSKGA EESRVRHKKH SSESPPGRDKG KLSRLKPAPP 900  
911 901 PPPAASAGKA GKPSQSPSQ EAAGEAVLGA KTKATSLVDA VNSDAAKPSQ PGEGLKQPVL 960  
912 961 PATPKPQSAK PSGTPIAP VPSTLPSASS ALAGDQPSST AFIPLISTRV SLRKRQPPE 1020  
913 1021 RIASGAIKKG VVLDSTEALC LAISRNSEQM ASHAVLEAG KNLYTFCVSY VDSIQQMRNK 1080  
914 1081 FAFREAINKL ENNRELQIC PATAGSGPAA TQDFSKLLSS VKEISDIVQR 1130

915

*Sequences for human and chicken Src, aligned using Clustal Omega*

916 SRC\_HUMAN 1 MGSNKSHPKD ASQRRRSLEP AENVHGAGGG AFPASQTPSK PASADGHRGP SAAFAPAAAE 60  
917 SRC\_CHICK 1 MGSSKSKPKD PSQRRRSLEP PDSTH--HG GFPASQTPNK TAAPDTHRTP SRSFGTVATE 57  
918 \*\*\*.\*\*\*\*\* \*\*\*\*\* :.\* \* .\*\*\*\*\*.\* \*: \* \* \* \* \* :.\* .\*: \*  
919 SRC\_HUMAN 61 PKLFGGFNSS DTVTSPQRAG PLAGGVTTFFV ALYDYESRTE TDLSFKKGER LQIVNNTTEGD 120  
920 SRC\_CHICK 58 PKLFGGFNTS DTVTSPQRAG ALAGGVTTFFV ALYDYESRTE TDLSFKKGER LQIVNNTTEGD 117  
921 \*\*\*\*\*.\* \*\*\*\*\* \*\*\*\*\* \*\*\*\*\* \*\*\*\*\* \*\*\*\*\* \*\*\*\*\*  
922 SRC\_HUMAN 121 WWLAHSLSTG QTGYIPSNYV APSDSIQAE WYFGKITRRE SERLLLNAEN PRGTFLVRES 180  
923 SRC\_CHICK 118 WWLAHSLTTG QTGYIPSNYV APSDSIQAE WYFGKITRRE SERLLNPNEN PRGTFLVRES 177  
924 \*\*\*\*\*.\* \*\*\*\*\* \*\*\*\*\* \*\*\*\*\* \*\*\*\*\* \*\*\*\*\* \*\*\*\*\*  
925 SRC\_HUMAN 181 ETTKGAYCLS VSDFDNAKGL NVKHYKIRKL DSGGFYITSR TQFNSLQQLV AYYSKHADGL 240  
926 SRC\_CHICK 178 ETTKGAYCLS VSDFDNAKGL NVKHYKIRKL DSGGFYITSR TQFSSLQQLV AYYSKHADGL 237  
927 \*\*\*\*\* \*\*\*\*\* \*\*\*\*\* \*\*\*\*\* \*\*\*\*\* \*\*\*\*\* \*\*\*\*\*  
928 SRC\_HUMAN 241 CHRLTTVCPT SKPQTQGLAK DAWAIPRESL RLEVKLQGC FGEVWMTWN GTTRVAIKTL 300  
929 SRC\_CHICK 238 CHRLTNVCPT SKPQTQGLAK DAWAIPRESL RLEVKLQGC FGEVWMTWN GTTRVAIKTL 297  
930 \*\*\*\*\*.\* \*\*\*\*\* \*\*\*\*\* \*\*\*\*\* \*\*\*\*\* \*\*\*\*\* \*\*\*\*\*  
931 SRC\_HUMAN 301 KPGTMSPEAF LQEAQVMKKL RHEKLVQLYA VVSEEPYIV TEYMSKGSLL DFLKGETGKY 360  
932 SRC\_CHICK 298 KPGTMSPEAF LQEAQVMKKL RHEKLVQLYA VVSEEPYIV TEYMSKGSLL DFLKGEMGKY 357  
933 \*\*\*\*\* \*\*\*\*\* \*\*\*\*\* \*\*\*\*\* \*\*\*\*\* \*\*\*\*\* \*\*\*\*\*  
934 SRC\_HUMAN 361 LRLPQLVDMA AQIASGMAYV ERMNYVHRDL RAANILVGEN LVCKVADFGL ARLIEDNEYT 420  
935 SRC\_CHICK 358 LRLPQLVDMA AQIASGMAYV ERMNYVHRDL RAANILVGEN LVCKVADFGL ARLIEDNEYT 417  
936 \*\*\*\*\* \*\*\*\*\* \*\*\*\*\* \*\*\*\*\* \*\*\*\*\* \*\*\*\*\* \*\*\*\*\*  
937 SRC\_HUMAN 421 ARQGAKFPIK WTAPEAALYG RFTIKSDVWS FGILLTELTT KGRVPYPMV NREVLQDQVER 480  
938 SRC\_CHICK 418 ARQGAKFPIK WTAPEAALYG RFTIKSDVWS FGILLTELTT KGRVPYPMV NREVLQDQVER 477  
939 \*\*\*\*\* \*\*\*\*\* \*\*\*\*\* \*\*\*\*\* \*\*\*\*\* \*\*\*\*\* \*\*\*\*\*  
940 SRC\_HUMAN 481 GYRMPCPPEC PESLHDLMCQ CWRKEPEERP TFEYLQAFLE DYFTSTEPQY QPGENL 536  
941 SRC\_CHICK 478 GYRMPCPPEC PESLHDLMCQ CWRKDPEERP TFEYLQAFLE DYFTSTEPQY QPGENL 533  
942 \*\*\*\*\* \*\*\*\*\* \*\*\*\*\*.\* \*\*\*\*\* \*\*\*\*\* \*\*\*\*\* \*\*\*\*\*